



Optical temperature sensing in Er^{3+} - Yb^{3+} codoped CaWO_4 and the laser induced heating effect on the luminescence intensity saturation

Wei Xu ^{a, b, *}, Ying Cui ^a, Yuwei Hu ^a, Longjiang Zheng ^a, Zhiguo Zhang ^{b, c}, Wenwu Cao ^{b, d}

^a School of Electrical Engineering, Yanshan University, Qinhuangdao 066004, China

^b Condensed Matter Science and Technology Institute, Harbin Institute of Technology, Harbin 150001, China

^c Laboratory of Sono- and Photo-Theranostic Technologies, Harbin Institute of Technology, Harbin 150001, China

^d Materials Research Institute, The Pennsylvania State University, Pennsylvania 16802, USA



ARTICLE INFO

Article history:

Received 4 May 2017

Received in revised form

31 July 2017

Accepted 1 August 2017

Available online 4 August 2017

Keywords:

Optical temperature sensing

Upconversion

Dopant concentration

Luminescence intensity saturation

ABSTRACT

CaWO_4 phosphors doping with different Er^{3+} and Yb^{3+} ion concentrations were synthesized through high temperature solid-state reaction technique. Excited by 980 nm laser, the influence of rare earth dopant concentration on the thermometry behavior of Er^{3+} green upconversion emissions was discussed via the fluorescence intensity ratio method. Superior temperature sensing ability could be achieved in CaWO_4 : 0.1 mol% Er^{3+} –3 mol% Yb^{3+} , the maximum sensitivity of which is about $1.05 \times 10^{-2} \text{ K}^{-1}$ at 439 K. Meanwhile, the pumping laser induced thermal effect on the saturation of upconversion emission intensity has been preliminarily studied. The temperature of the irradiation spot on sample caused by the exposure of excitation laser is observed to be greatly enhanced as the pumping power increased. Based on the steady-state rate equations and the temperature dependence of luminescence decay curves, theoretical calculations have been performed. The results confirm that the laser induced heating effect plays an important role in the luminescence intensity saturation phenomenon.

© 2017 Published by Elsevier B.V.

1. Introduction

Temperature is one of the fundamental physical parameters and the realization of accurate and reliable temperature measurement is always a challenging task. Nowadays, much attention has been paid to the non-contact temperature sensors based on the rare earth (RE) ions activated luminescent materials, which present efficient luminescence, high sensitivity, good accuracy, and easy integration [1–3]. And the temperature could be measured through analyzing the fluorescence intensity, band shape, lifetimes, etc. Since the luminescence characteristics of the RE ions strongly depend on the temperature [4–6]. This contactless and non-invasive thermometry technique has little effect on the thermal state of detected objects and exhibit wide applications in many fields, such as chemistry, electromagnetism, and biomedicine, where conventional sensors can not be used. As one of the sensing methods, the fluorescence intensity ratio (FIR) technique is extensively regarded as a promising tool for mapping temperature

because the FIR from the thermally coupled levels (TCL) of RE ions is independent of spectrum losses and fluctuations in the excitation intensity [6]. Thus, reasonable measurement accuracy and sensitivity could be obtained with this method, and several RE ions have already been explored for the FIR related temperature survey [7–10]. Among these ions, Er^{3+} is the most well studied, which has the TCL of ${}^4\text{S}_{3/2}$ and ${}^2\text{H}_{11/2}$ with proper energy separation as well as the corresponding strong green upconversion (UC) photoluminescence under near-infrared (NIR) light excitation [11,12]. And owing to the large absorption cross-section around NIR region, Yb^{3+} is usually utilized as the sensitizer to further enhance Er^{3+} UC emissions. The NIR laser excited Er^{3+} - Yb^{3+} codoped systems have been widely considered as promising candidates for surface temperature detection and biological thermal probes with preferable measurement accuracy and resolution [13–15]. On the other hand, host material is also a critical element determining the sensing performance because the ion's optical properties are ruled by the coordination environment. Recently, tungstates have attracted much interest due to their distinguished features, including good thermal stability, high density, as well as low phonon threshold energy, which enable the activators to emit stable and intense luminescence even at high temperatures [16–18]. Meanwhile, the

* Corresponding author. School of Electrical Engineering, Yanshan University, Qinhuangdao 066004, China.

E-mail address: college_d@163.com (W. Xu).

study on the thermal sensing behavior of Er^{3+} - Yb^{3+} codoped tungstates is also increasing. Lu et al. pointed out that excellent temperature sensing properties could be achieved based on the stark sublevels of Er^{3+} - Yb^{3+} codoped $\text{Gd}_2(\text{WO}_4)_3$ phosphor [19]. Chai et al. observed color-tunable UC emissions in Er^{3+} - Yb^{3+} codoped ZnWO_4 and a thermometry sensitivity of 0.0099 K⁻¹ was obtained in such compound [20]. Moreover, it was reported that the UC luminescence efficiency of $\text{NaLa}(\text{WO}_4)_2$: Er^{3+} - Yb^{3+} is comparable to that of $\beta\text{-NaYF}_4$: Er^{3+} - Yb^{3+} but with a much higher thermal sensitivity than that of the fluoride [21]. Despite the significant progress in luminescent thermometry, many applications define additional requirement, especially the enhanced measurement sensitivity and precision. As is well known, the doping levels of RE ions have appreciable influence on their luminescence characteristics, i.e., the temperature response properties of Er^{3+} green emissions could be improved through designing the dopant concentration of Er^{3+} and Yb^{3+} ions. Thus, to further develop Er^{3+} luminescence based temperature sensors, it is of technological and scientific importance to comprehend the effect of RE content on the thermometry behavior in Er^{3+} - Yb^{3+} codoped tungstate matrix, which, to our best knowledge, is still lacking.

Additionally, the pumping power dependence of emission intensities is known to be very essential for understanding the excitation mechanisms in UC luminescence materials. And it is usually assumed that the order n of the UC process, i.e. the number of the pumping photons required to excite the emitting states, is indicated by the slope of the luminescence intensity I vs. pumping power P in double-logarithmic representation. In many works, it has been observed that the dependence of the UC emission intensity on pumping power decreases in slope with the strength of excitation [22–27]. This phenomenon is considered as luminescence intensity saturation (LIS). Some works have been performed to interpret the mechanisms leading to such phenomenon, and most believe the competition between the linear decay and the UC process of the intermediate excited states results in the LIS [22–27]. Generally, it would be hard for the UC process to transcend the linear decay when excited by a continuous wave laser with hundreds of milliwatt. In fact, the laser energy absorbed by the RE ions is not only used to generate the luminescence, but also introduce heat into the sample. And the temperature for the irradiation spot on the sample would rise as the laser power is strengthened. This heating effect is more obvious for the phosphors because of the poor thermal conductivity and the opacity [9,28]. The temperature increment could subsequently cause the changing in the phonon-involved behaviors, including the multi-phonon nonradiative relaxation, phonon-assisted energy transfer, and phonon-assisted energy absorbance. These processes will influence the population of the excited levels of RE ions and might contribute to the UC LIS. However, up to now, few works has taken the laser induced heating (LH) effect into account when discussing the LIS for the upconverted materials.

In this work, CaWO_4 was selected as the studied object, and a series of Er^{3+} - Yb^{3+} codoped CaWO_4 phosphors were prepared. The influence of Er^{3+} and Yb^{3+} doping concentration on Er^{3+} green emissions based thermometry behavior was investigated when excited by 980 nm laser. Meanwhile, the LH effect on the LIS phenomenon was studied based on Er^{3+} - Yb^{3+} codoped CaWO_4 phosphors. The results illustrate that enhancing Yb^{3+} or reducing Er^{3+} dopant content can modify the luminescence thermometry ability in Er^{3+} - Yb^{3+} codoped CaWO_4 . Besides, the LH effect is proven to play an important role in the LIS phenomenon.

2. Experimental

The CaWO_4 phosphors codoping with 0.5 mol% Er^{3+} - x mol%

Yb^{3+} ($x = 0, 1, 3, 5$) and those with x mol% Er^{3+} ($x = 0.1, 0.3, 0.5, 0.7$) - 3 mol% Yb^{3+} were prepared with the high temperature solid-state method. The starting materials were CaCO_3 (99.99%, Aladdin), WO_3 (99.99%, Aladdin), Er_2O_3 (99.99%, Aladdin), and Yb_2O_3 (99.99%, Aladdin). The raw powders with the designed stoichiometry were fully mixed and grinded. Then the mixtures were put into the corundum crucibles and sintered in a furnace for 10 h at 1300 °C in air. The obtained Er^{3+} - Yb^{3+} codoped CaWO_4 phosphors were finally pressed into a thin disk with a diameter of 1.3 cm. A powder diffractometer (Rigaku DMAX2500) using $\text{Cu K}\alpha$ radiation ($\lambda = 0.154$ nm) was applied to confirm the crystal phase through X-ray diffraction (XRD) method. The measurement angular is in the range of $10^\circ \leq 2\theta \leq 80^\circ$ with a step size of 0.02° and speed of $12^\circ/\text{min}$. To estimate the particle size and morphology of the crystalline powder, Hitachi S4800 scanning electron microscopy (SEM) was used. The samples are excited by a 980 nm continuous wave diode laser, which is fitted on a laser diode (LD) mount and linked to a Thorlabs ITC4005 LD/temperature controller. Zolix-SBP300 grating spectrometer equipped with a CR131 photomultiplier is used to record the luminescence spectra. The temperature of the samples is controlled by the experimental system reported in our previous work [18]. The luminescence decay curves are measured by 980 nm laser modulated through square-wave electric current and recorded by Tektronix DPO 5054 oscilloscope. To guarantee the validity of the experimental results, the position for the optical devices keeps unchanged during the whole experiment.

3. Results and discussion

3.1. Optical temperature sensing behavior

The XRD patterns for the pure CaWO_4 and Er^{3+} - Yb^{3+} codoped CaWO_4 phosphors are shown in Fig. 1(a). To clearly exhibit the changing in the XRD patterns, intense diffraction peaks in the range of $15^\circ \leq 2\theta \leq 64^\circ$ were depicted. All of the diffraction peaks for the as-prepared samples can be well indexed to the tetragonal structure of CaWO_4 based on the PDF card # 77–2236, and no other diffraction peaks were detected, indicating the dopants (Er^{3+} and Yb^{3+} ions) are successfully incorporated into the host lattice and do not cause significant changes to the crystal structure. Meanwhile, stronger diffraction at 2θ values around 18.8° (101) and 28.6° (112) obviously exhibits red-shift with the increasing of Er^{3+} and Yb^{3+} content. The diffraction peak around 18.8° is shown in Fig. 1(b) to clearly present the red-shift phenomenon. When RE ions are incorporated into the lattice of CaWO_4 , they usually substitute Ca^{2+} ions in the dodecahedral sites with the generation of cation vacancies for charge compensation. The substitution of Ca^{2+} ions possessing larger radius (~1.12 Å) by Er^{3+} (~1.00 Å) and Yb^{3+} (~0.98 Å) with smaller radii would result in the shrinkage of the host lattice [29,30]. Through the SEM image (see Fig. S1 in supplementary material), it can be seen that the phosphors consist of aggregated and irregular particles, and size of distinguishable particles is in the micron range. To understand the dopant effect of Er^{3+} and Yb^{3+} on Er^{3+} green luminescence based thermometry properties, the UC emission spectra are recorded at temperatures ranging from 307 to 773 K. To avoid the laser thermal effect on the below calibration, the excitation power of 980 nm LD is set as low as 50 mW. Figs. 2 and 3 present the temperature dependent green UC emission spectra for 0.5 mol% Er^{3+} - x mol% Yb^{3+} ($x = 0, 1, 3, 5$) and x mol% Er^{3+} ($x = 0.1, 0.3, 0.5, 0.7$) - 3 mol% Yb^{3+} codoped samples. Two dominant emission bands of Er^{3+} centered around 530 and 553 nm are attributed to the transitions of $^2\text{H}_{11/2} \rightarrow ^4\text{I}_{15/2}$ and $^4\text{S}_{3/2} \rightarrow ^4\text{I}_{15/2}$, respectively. And the corresponding FIR between 530 and 553 nm luminescence ($I_{\text{H}}/I_{\text{S}}$) at different temperatures are also included in the figures. Obviously, the emission band positions are

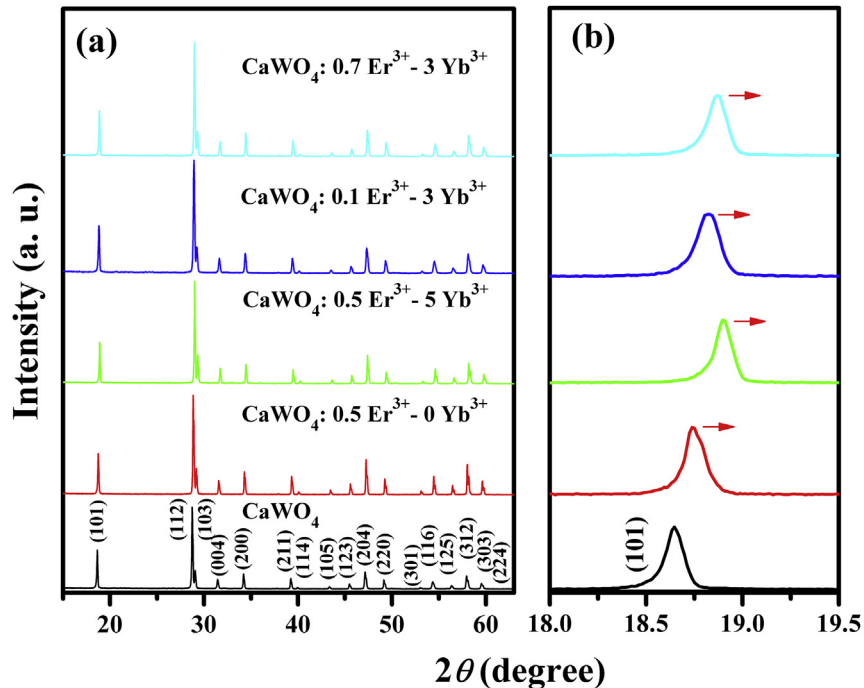


Fig. 1. XRD patterns for the CaWO₄ phosphors and CaWO₄ doping with different Er³⁺ and Yb³⁺ concentrations.

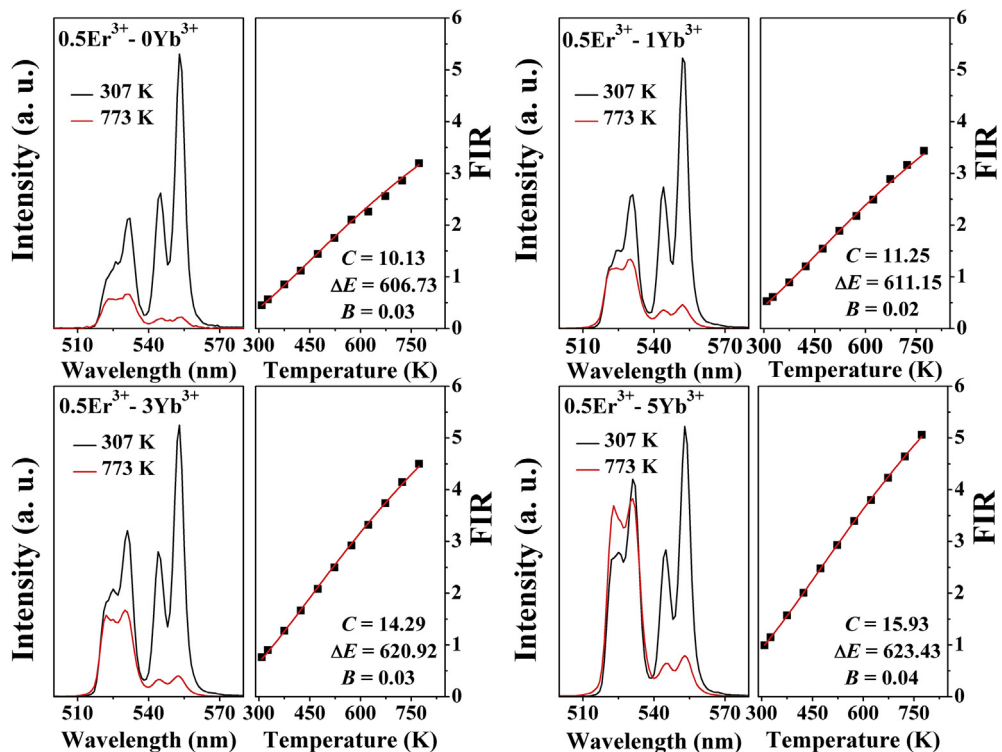


Fig. 2. Green UC emission spectra for CaWO₄: 0.5 mol% Er³⁺-x mol% Yb³⁺ ($x = 0, 1, 3, 5$) as well as the FIR plotted as a function of temperature.

observed to scarcely change as temperature rises, but the FIR has varied with the increase of temperature. This is mainly ascribed to the fact that the relative population between the thermally coupled levels follows Boltzmann type distribution. According to the theory by Wade et al., the FIR of the emissions from TCL of Er³⁺ ions is modified as [6].

$$FIR \equiv \frac{I_H}{I_S} = \frac{A_H g_H \sigma_H \omega_H}{A_S g_S \sigma_S \omega_S} \exp\left(-\frac{\Delta E}{k_B T}\right) + B = C \exp\left(-\frac{\Delta E}{k_B T}\right) + B, \quad (1)$$

where I_H and I_S are respectively the relative luminescence intensity

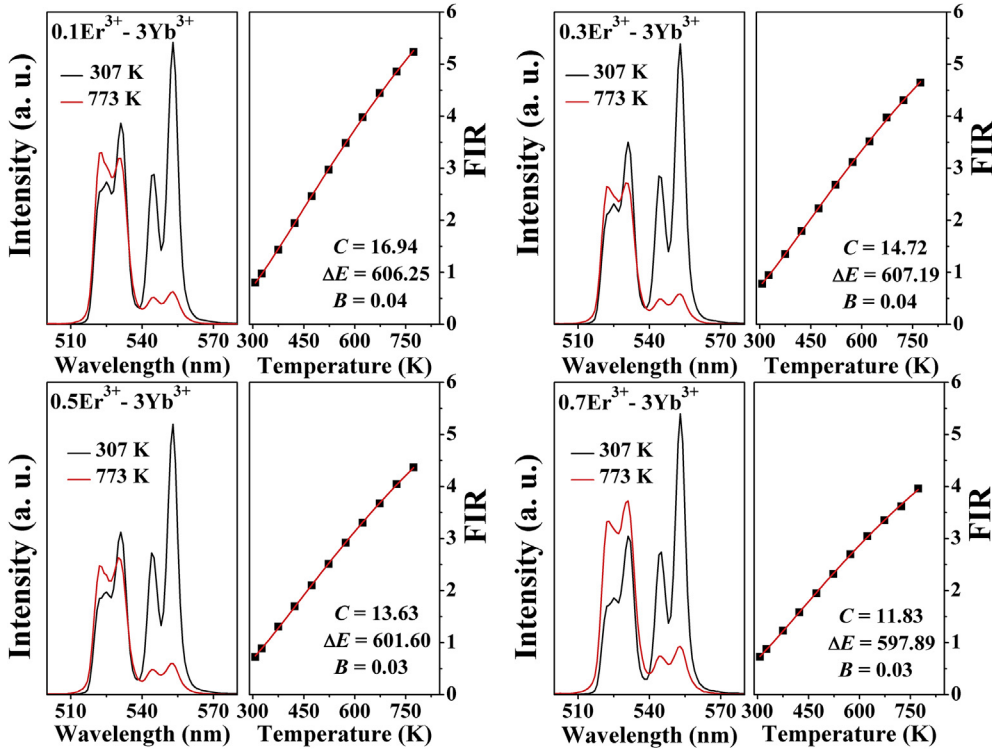


Fig. 3. Green UC emission spectra for CaWO_4 : x mol% Er^{3+} -3 mol% Yb^{3+} ($x = 0.1, 0.3, 0.5, 0.7$) as well as the FIR plotted as a function of temperature.

originated from the upper and lower TCL of Er^{3+} ; A and g represent the spontaneous transition rate and the degeneracy; σ is the detection system response at the angular frequency ω ; ΔE is the energy gap between the TCL; C and B are constants, and k_B and T denote the Boltzmann constant and the absolutely temperature, respectively. The fitted results in Figs. 2 and 3 show that the fittings all match well with the experimental values and the fitted coefficients ΔE and B barely change with the variation of RE concentration. While it is interesting to note that the pre-exponential parameter clearly changes in different samples. For 0.5 mol% Er^{3+} - x mol% Yb^{3+} codoped CaWO_4 , the value of C is gradually enhanced from 10.13 to 15.93 as Yb^{3+} concentration is increased. In contrast, the reduction of C from 16.94 to 11.83 is observed with the increment of Er^{3+} ions in x mol% Er^{3+} - 3 mol% Yb^{3+} codoped ones. Several testing cycles were performed, and a good reproducibility of the thermometry technique was obtained (see Fig. S2 in the supplementary material), which benefits from the excellent thermal stability of the phosphors evidenced by the FIR and XRD analysis (see Figs. S3 and S4 in the supplementary material).

As for the thermometry, the measurement sensitivity is an important parameter reflecting the changing rate of FIR with temperature, which is defined as [13].

$$S \equiv \frac{d\text{FIR}}{dT} = \frac{A_H g_H \sigma_H \omega_H}{A_S g_S \sigma_S \omega_S} \exp\left(-\frac{\Delta E}{k_B T}\right) \times \frac{\Delta E}{k_B T^2}. \quad (2)$$

The sensitivities obtained from the samples are presented in Fig. 4. At the same temperature, the sensitivity is evidently enhanced with Yb^{3+} content, whereas decreased as Er^{3+} dopant is raised. Through Eq. (2), it is known that the sensitivity is dominated by A , g , σ , ω , and ΔE at certain temperature. And the parameters g , σ , ω , and ΔE should be identical at different samples. Nevertheless, the spontaneous transition rates and the spectral features of the Er^{3+} - Yb^{3+} codoped oxides are sensitive to the cationic environment and ratio between the particular RE dopants [31–33]. And as shown in

Fig. 1(b), the increment doping concentration of Er^{3+} and Yb^{3+} could arouse slight changing in the host lattice. And the minor alteration in the local environment of activator would induce significant variation in the spontaneous transition rates, consequently modulating the A_H/A_S . From the results given in Figs. 2 and 3, it is assumed that the value of A_H/A_S for Er^{3+} is enlarged with increasing Yb^{3+} dopant but changed from the negative relationship with Er^{3+} content in CaWO_4 . The changing of A_H/A_S with Er^{3+} and Yb^{3+} dopants can be distinctly inferred from the room-temperature UC emission spectra. At room temperature, the emission band centered around 530 nm has been relatively weakened compared with that of 553 nm when increasing Er^{3+} concentration, and the opposite changing trend is observed by enhancing Yb^{3+} doping content. Such changing style could be clearly exhibited by the normalized ratios among the A_H/A_S values, which are estimated to be about 1: 1.18: 1.56: 1.91 for 0.5 mol% Er^{3+} - x mol% Yb^{3+} ($x = 0, 1, 3, 5$) codoped CaWO_4 and 1: 0.89: 0.81: 0.76 for x mol% Er^{3+} - 3 mol% Yb^{3+} ($x = 0.1, 0.3, 0.5, 0.7$) ones. And it is worthwhile to note that similar changing trend of A_H/A_S can also be found in $\text{Er}^{3+}/\text{Yb}^{3+}$ codoped glasses [34]. On the other hand, raising Yb^{3+} concentration would increase the absorption coefficient of samples around 1000 nm, which is in favor of enhancing Er^{3+} UC emissions and also contributes to the increment of C value. And increasing Er^{3+} content most probably results in the concentration quenching caused by cross-relaxation, which would also lead to the decrease in C value. The variation in the C consequently provides different measurement sensitivity. The maximum sensitivity is achieved in 0.1 mol% Er^{3+} - 3 mol% Yb^{3+} codoped CaWO_4 , which is about $1.05 \times 10^{-2} \text{ K}^{-1}$ at 439 K. Furthermore, the measurement error can be estimated from the calculated sensitivity [35].

$$\Delta T = \frac{\Delta \text{FIR} k_B T^2}{\text{FIR} \Delta E} = \frac{\Delta \text{FIR}}{S}. \quad (3)$$

When a signal division circuitry with the same precision is

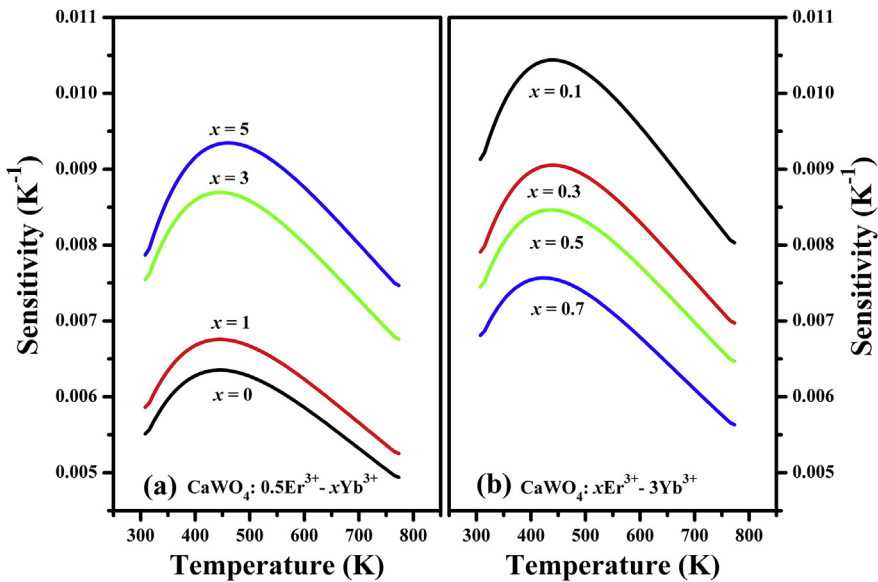


Fig. 4. The measurement sensitivities for Er^{3+} - Yb^{3+} codoped CaWO_4 phosphors.

applied, the high sensitivity is in favor of getting small error. Compared with other Er^{3+} activated thermometers given in Table 1, excellent thermometry ability could be expected by using CaWO_4 : 0.1 mol% Er^{3+} -3 mol% Yb^{3+} phosphor. And it is interesting to observe that the thermometry based on Er^{3+} - Yb^{3+} codoped tungstate possesses higher sensitivities. Especially for the MWO_4 : Er^{3+} - Yb^{3+} ($M = \text{Ca}^{2+}, \text{Sr}^{2+}, \text{Mg}^{2+}, \text{Zn}^{2+}$), as RE ions are incorporated into the matrix lattice to substitute M ions, the crystal structure could be efficiently distorted by such substitution due to the different ion radius and valent mismatch. This behavior is particularly in favor of the radiation from $^2\text{H}_{11/2} \rightarrow ^4\text{I}_{15/2}$ hypersensitive transition and leads to higher temperature measurement sensitivity [14]. Furthermore, through the changing tendency of $A_{\text{H}}/A_{\text{S}}$ with Er^{3+} and Yb^{3+} concentration, thermometry sensitivity and accuracy can be further improved by modifying the dopants of Er^{3+} and Yb^{3+} in CaWO_4 . Yet, careful optimization is necessary to balance the CR quenching, signal to noise ratio, and sensitivity/accuracy issues. Meanwhile, considering the strong dependence of multi-photon excitation process on the pumping power, attention should also be paid to the power adjusting during the temperature measurement since overlarge excitation power might induce absorption

saturation and produce thermal effect, influencing the thermometry behavior [44,45].

3.2. Laser induced heating effect on the luminescence intensity saturation

The optical thermometry based on the FIR is known to be an effective tool to determine the pumping laser induced heating (LH) effect on the sample [28,46]. In the following, the LH effect on the LIS is to be studied based on CaWO_4 : Er^{3+} - Yb^{3+} since the LIS phenomenon has been widely observed in Er^{3+} / Yb^{3+} codoped systems [23–27]. And considering the complex UC mechanisms involved in Er^{3+} - Yb^{3+} codoped systems, CaWO_4 doping with small Er^{3+} and Yb^{3+} contents (0.1 mol% Er^{3+} -1 mol% Yb^{3+} synthesized in Ref. [18]) is chosen as the studied object to simplify the subsequent discussion. The UC emission spectra at different excitation powers are recorded and the temperature of the laser spot on the sample is estimated based on the FIR method, as shown in Fig. 5. To clearly present the change of spectra profile with the excitation power, the luminescence intensity has been normalized according to that of 553 nm emission. It can be seen that the laser spot temperature has

Table 1

Thermometry properties for the optical temperature sensors based on the green UC emissions of Er^{3+} and Er^{3+} - Yb^{3+} codoped compounds.

Materials	Temperature range (K)	Excitation wavelength (nm)	Maximum sensitivity (K^{-1})	Reference
$\text{Na}_{0.5}\text{Gd}_{0.5}\text{MoO}_4$: Er^{3+} - Yb^{3+}	298–778	980	0.0086	[8]
$\text{Y}_2\text{Ti}_2\text{O}_7$: Er^{3+} - Yb^{3+}	298–673	980	0.0067	[11]
La_2O_3 : Er^{3+} - Yb^{3+}	303–600	980	0.0091	[12]
$\text{Yb}_2\text{Ti}_2\text{O}_7$: Er^{3+} - Mo^{6+}	295–973	980	0.0048	[13]
Oxyfluoride glass: Er^{3+}	293–720	488	0.0066	[14]
NaYTiO_4 : Er^{3+} - Yb^{3+}	300–510	980	0.0045	[15]
ZnWO_4 : Er^{3+} - Yb^{3+}	83–583	980	0.0099	[20]
$\text{NaLa(WO}_4)_2$: Er^{3+} - Yb^{3+}	139–468	980	0.0115	[21]
$\text{CaAl}_2\text{ZnO}_5$: Er^{3+} - Yb^{3+}	298–513	980	0.0059	[36]
$\text{Na}_2\text{Gd}_2\text{Ti}_3\text{O}_{10}$: Er^{3+} - Yb^{3+}	290–490	980	0.0058	[37]
$\text{Na}_{0.5}\text{Bi}_{0.5}\text{TiO}_3$: Er^{3+}	80–480	980	0.0053	[38]
GdVO_4 : Er^{3+} - Yb^{3+}	307–473	980	0.0085	[39]
MgWO_4 : Er^{3+} - Yb^{3+}	163–583	980	0.0093	[40]
SrWO_4 : Er^{3+} - Yb^{3+}	95–775	980	0.0128	[41]
SrMoO_4 : Er^{3+} - Yb^{3+}	93–773	980	0.0128	[42]
$\text{NaY(WO}_4)_2$: Er^{3+} - Yb^{3+}	133–773	980	0.0112	[43]
CaWO_4 : Er^{3+} - Yb^{3+}	303–773	980	0.0105	This Work

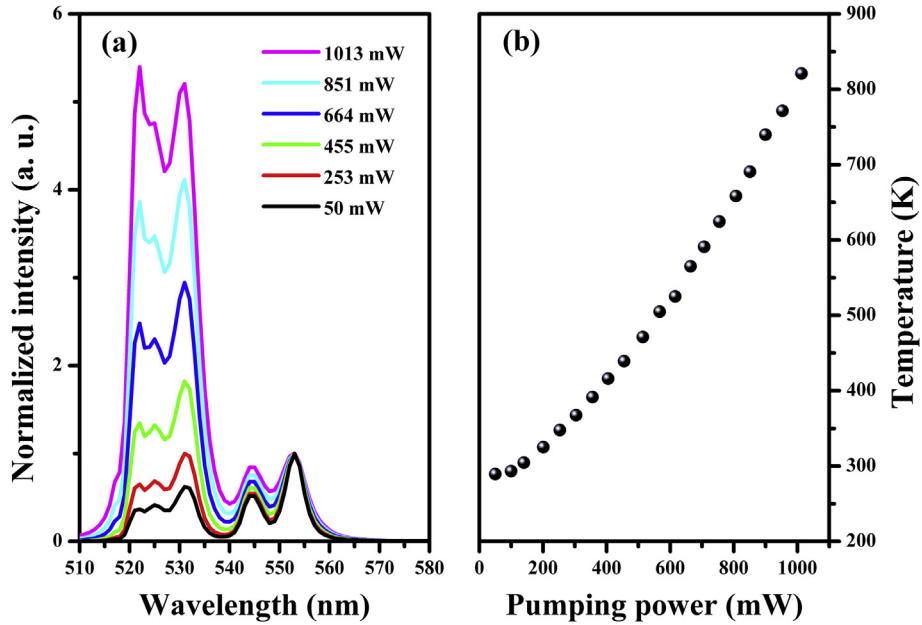


Fig. 5. (a) Normalized spectra of the green UC emissions at different excitation powers and (b) the calculated local temperature for Er^{3+} - Yb^{3+} codoped CaWO_4 under 980 nm laser excitation.

been significantly enhanced as the power increases. To further understand the LH influence on the population of the excited states, the steady-state rate equations need to be listed.

It is known that under 980 nm laser excitation, the excited levels of Er^{3+} can be populated both by energy transfer (ET) from Yb^{3+} to Er^{3+} and its own ground state absorption (GSA) as well as the excited state absorption (ESA). But the population through GSA and ESA could be neglected compared with that through the ET processes (see Fig. S5 in the supplementary material). And considering the small doping concentration of Er^{3+} , the cross-relaxations between Er^{3+} are also neglected. Then, the rate equations describing the excitation mechanisms can be written as follows

$$\frac{dN_1}{dt} = C_0 N_b N_0 - \frac{N_1}{\tau_1} - C_1 N_b N_1 \quad (4)$$

$$\frac{dN_2}{dt} = C_1 N_b N_1 - \frac{N_2}{\tau_2} - I N_2 \quad (5)$$

$$\frac{dN_3}{dt} = I N_2 - N_3 / \tau_3 \quad (6)$$

$$\frac{dN_b}{dt} = \frac{\varepsilon N_a \lambda_p P}{hcs} - C_0 N_b N_0 - C_1 N_b N_1 - \frac{N_b}{\tau_{Yb}} \quad (7)$$

where N_0 , N_1 , N_2 , N_3 , N_a , N_b are the population densities on Er^{3+} : $^4\text{I}_{15/2}$, $^4\text{I}_{11/2}$, $^4\text{S}_{3/2}$, $^2\text{H}_{11/2}$, $^2\text{F}_{5/2}$ states, respectively; τ_1 , τ_2 , τ_3 , τ_{Yb} are the lifetimes for Er^{3+} : $^4\text{I}_{11/2}$, $^4\text{S}_{3/2}$, $^2\text{H}_{11/2}$, and Yb^{3+} : $^2\text{F}_{7/2}$, $^2\text{F}_{5/2}$ states, respectively; C_0 and C_1 are the ET coefficients; I is the thermally populating rate from $^4\text{S}_{3/2}$ to $^2\text{H}_{11/2}$; λ_p and ε represent the pump wavelength (980 nm) and the absorption cross section of Yb^{3+} at 980 nm; P and s are the power and the square of the irradiation spot, respectively; h and c represent the Planck constant and light speed, respectively. The detailed description can be consulted in Fig. 6. Eqs. (5) and (6) are obtained based on the assumption: because of the much weak luminescence from the $^4\text{F}_{7/2}$ of Er^{3+} as well as little luminescence from $^2\text{H}_{11/2} \rightarrow ^4\text{I}_{15/2}$ at low

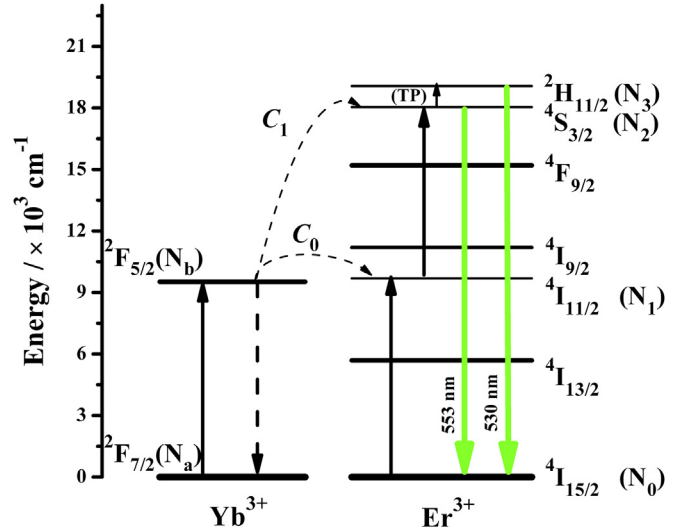


Fig. 6. The energy level diagrams for Yb^{3+} and Er^{3+} as well as the UC mechanism (TP = Thermal population).

temperature, it is rational to deem that ions on the $^4\text{F}_{7/2}$ state decays simply nonradiatively to the $^4\text{S}_{3/2}$ state [47]. So it can be considered that the population of $^4\text{S}_{3/2}$ is directly originated from the ET process: Yb^{3+} : $^2\text{F}_{5/2}$ + Er^{3+} : $^4\text{I}_{11/2}$ → Yb^{3+} : $^2\text{F}_{7/2}$ + Er^{3+} : $^4\text{S}_{3/2}$ [47,48]. And the population of $^2\text{H}_{11/2}$ is totally attributed to the thermal population from $^4\text{S}_{3/2}$ due to their thermally coupled relationship [47]. Under steady-state excitation, Eqs. (4)–(7) give rise to the population of $^4\text{S}_{3/2}$ emitting level as

$$N_2 = \frac{\alpha}{\gamma^2} \times \frac{P^2}{(1/\tau_2 + \Gamma)/\tau_1} \quad (8)$$

where $\alpha = C_1 C_0 N_0 N_a^2 \varepsilon^2 \lambda_p^2 / h^2 c^2 s^2$; $\gamma = C_0 N_0 + \tau_{Yb}^{-1}$ (detailed calculation routine can be consulted in the supplementary material). In view of the Boltzmann type distribution between $^2\text{H}_{11/2}$ and $^4\text{S}_{3/2}$ levels, Γ

is obtained by combining Eq. (6) as

$$I = \frac{g_H}{g_S \tau_3} \exp\left(-\frac{\Delta E}{k_B T}\right) \quad (9)$$

In order to get the result in Eq. (8), it has been assumed that the ET between the acceptor and donor do not significantly affect the lifetime of the excited ions, implying $\tau_1^{-1} \gg C_1 N_b$, i.e. the UC process for the discussed level is neglected. Pumped by a continuous diode laser with low power, just a few ions can be excited, implying N_x ($x=0, a$) \approx const. and $C_0 N_0 \gg C_1 N_1$.

It is known that the lifetimes for the excited levels can be described as [49].

$$\frac{1}{\tau} = \sum A_{ij} + W_{NR} = \sum A_{ij} + W_0 \left[1 - \exp\left(-\frac{\hbar\omega}{k_B T}\right) \right]^{-p} \quad (10)$$

where $\sum A_{ij}$ is the sum of radiative transition rates from level i to its lower lying levels j ; W_{NR} and W_0 are the multiphonon nonradiative relaxation (MNR) rate and MNR at 0 K; $\hbar\omega$ and p denote the phonon energy and the number of phonons involved in the MNR, respectively. The MNR for $\text{Yb}^{3+}: {}^2\text{F}_{5/2}$ state is not expected due to the large energy gap between ${}^2\text{F}_{5/2}$ and ${}^2\text{F}_{7/2}$. The MNR for $\text{Er}^{3+}: {}^4\text{I}_{11/2}$ state is neglected for simplifying the discussion. Meanwhile, because of the resonant ET from Yb^{3+} to Er^{3+} when excited by 980 nm laser, C_0 and C_1 are assumed as constants without lack of generality. Based on these above assumptions, τ_1 , α , and γ in Eq. (8) can be considered as constants. If the laser heating effect, i.e. the temperature dependent parameters τ_2 and Γ in Eq. (8) are negligible, the result $N_2 \propto P^2$ (i.e. $n = 2$) can be obtained, as seen the ideal value in Fig. 7. However, owing to the giant enhancement of the irradiation spot temperature on the sample with the increase of excitation power, the thermal absorption and the MNR processes will be promoted, which make the values of τ_2^{-1} , τ_3^{-1} and Γ become larger and finally contribute to the depopulation of ${}^4\text{S}_{3/2}$ state. Hence, the LH effect is taken into consideration in the present work.

It can be known from Eqs. (8)–(10) that the constants α and γ do not influence the slope n of the luminescence intensity vs. pumping power in double-logarithmic representation. Therefore, n can be quantitatively calculated if τ_2^{-1} and τ_3^{-1} at temperatures corresponding to the different pumping powers are given. For this purpose, the temperature dependent luminescence decay curves for

${}^4\text{S}_{3/2}$ and ${}^2\text{H}_{11/2}$ states have been measured, as shown in the left of Fig. 8. The corresponding decay rates are obtained based on these curves and fitted by Eq. (10), as shown in the right of Fig. 8. It can be observed that the fitted curves agree well with the experimental data. τ_2^{-1} and τ_3^{-1} at temperatures corresponding to the different pumping powers are deduced through the fitted results. Noting the emission intensity I is proportional to N , the slope n is calculated based on the above theory model and presented as theoretical value-I in Fig. 7. The theoretically calculated slopes n are observed to agree well with the experimental results in the pumping powers ranging from 50 to 570 mW. The decrease of n (1.10) for the experimental data in the range of 300–570 mW implies the occurrence of LIS, which can also be inferred via the theoretical calculation (1.21) based on our rate equation model. As the power is further increased (>570 mW), the n value for the experimental data turns into a negative value due to the thermal quenching. Although the n for the theoretical value-I keeps decreasing at powers surpassing 570 mW, the corresponding value is larger than that in the experiment. This deviation is probably attributed to the neglecting of the MNR for the intermediate level ${}^4\text{I}_{11/2}$ during the analysis. Owing to the great enhancement of laser spot temperature with the increase of the excitation powers, the MNR process for the intermediate state ${}^4\text{I}_{11/2}$ will also take place and be strengthened, which naturally weakens the population on $\text{Er}^{3+}: {}^4\text{S}_{3/2}$ state and consequently contribute to the thermal quenching for the luminescence at high pumping powers. Here, it would be interesting to separately understand how the MNR process influences LIS. The effect of the MNR for $\text{Er}^{3+}: {}^4\text{I}_{11/2}$ is deduced and taken into account by the ratio I_e/I_t between the relative intensities corresponding to the experimental data I_e and theoretical value-I I_t . The Γ item in Eq. (8) is temporarily discarded, and the relationship between the 553 nm emission intensity I and the excitation power P could be written as follow

$$I = \frac{\alpha}{\gamma^2} \times \frac{P^2}{1/(\tau_1 \tau_2)}. \quad (11)$$

The calculated slopes n are shown as theoretical value-II in Fig. 7. It is depicted that the LIS can be obviously induced only by the thermally strengthened MNR as the pumping power is increased.

Based on Eqs. (8)–(11) and the results shown in Fig. 5, the relationship between the emission intensity I and the excitation power P can be generally expressed as

$$I \propto \frac{P^n}{f(P)} \quad (12)$$

where $f(P)$ is a function of excitation power P , reflecting the laser induced thermal effect, and the value of $f(P)$ would increase as P is raised. From the results presented in Fig. 7, some conclusions could be achieved. When the pumping power P is relatively low, the laser induced heating effect is not obvious. Therefore, $f(P)$ is negligible compared to P^n , so we can approximately get $I \propto P^n$. With the increase of P , $f(P)$ is comparable to P^n , getting the n to become smaller and leading to the LIS phenomenon. As P is further enhanced, $f(P)$ becomes larger than P^n , causing the decrease of I with the increase of P and finally resulting in the luminescence thermal quenching.

4. Conclusions

CaWO_4 phosphors doping with different Er^{3+} and Yb^{3+} concentrations were prepared, and the influence of RE dopant content on the thermometry behavior of Er^{3+} green UC emissions was discussed when excited by 980 nm cw diode laser. A maximum sensitivity of $1.05 \times 10^{-2} \text{ K}^{-1}$ is achieved here, which is superior to

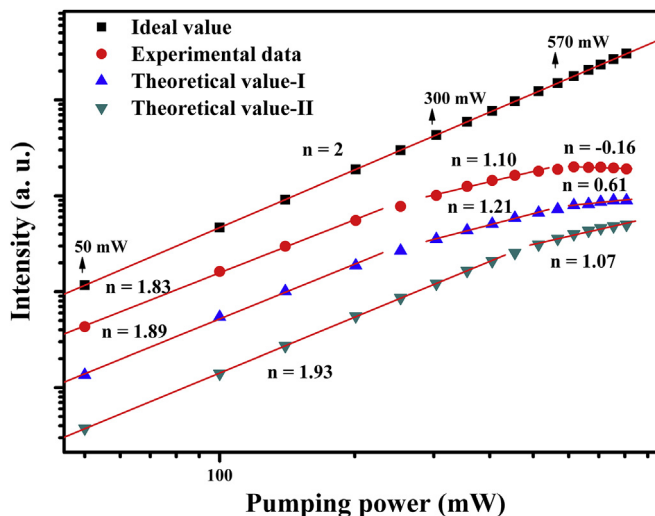


Fig. 7. The experimental and theoretical slope of the intensity for 553 nm emission vs. the pumping power in double-logarithmic representation.

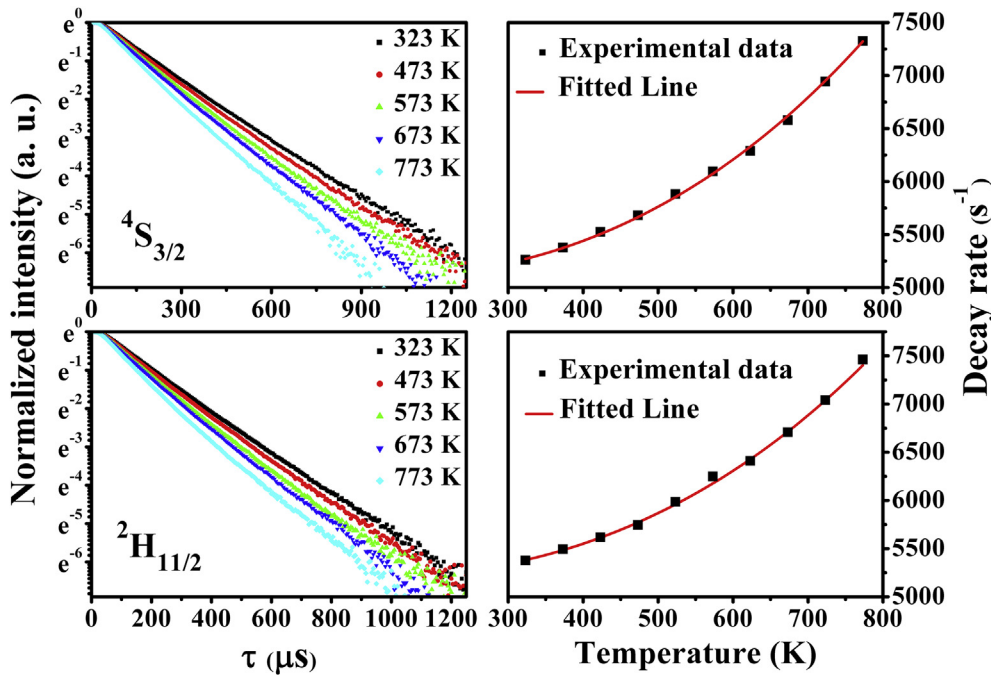


Fig. 8. The luminescence decay curves and decay rates for the $^4\text{S}_{3/2}$ and $^2\text{H}_{11/2}$ states at different temperatures as well as the fitting results.

other Er^{3+} based sensors. And the result implies that preferable temperature sensing properties could be realized by further raising Yb^{3+} or reducing Er^{3+} dopants. In addition, the excitation laser induced heating effect in Er^{3+} - Yb^{3+} codoped CaWO_4 has been studied by using the luminescence thermometry method. It is illustrated that such heating effect plays an important role in the UC luminescence intensity saturation and should be taken into consideration when investigating the excitation mechanisms for the upconverted materials.

Acknowledgements

This work was supported by the National Nature Science Foundation of China (NSFC) (grant number 61505174); and the Hebei Province Nature Science Foundation (grant number E2016203185).

Appendix A. Supplementary data

Supplementary data related to this article can be found at <http://dx.doi.org/10.1016/j.jallcom.2017.08.007>.

References

- [1] T.T. Bai, N. Gu, Micro/Nanoscale thermometry for cellular thermal sensing, *Small* 12 (2016) 1590–1610.
- [2] S.N. Zhao, L.J. Li, X.Z. Song, M. Zhu, Z.M. Hao, X. Meng, L.L. Wu, J. Feng, S.Y. Song, C. Wang, Lanthanide ion codoped emitters for tailoring emission trajectory and temperature sensing, *Adv. Funct. Mater.* 25 (2015) 1463–1469.
- [3] E.C. Ximenes, W.Q. Santos, U. Rocha, U.K. Kagola, F. Sanz-Rodríguez, N. Fernández, A.D.S. Gouveia-Neto, D. Bravo, A.M. Domingo, B. del Rosa, Unveiling in vivo subcutaneous thermal dynamics by infrared luminescent nanothermometers, *Nano Lett.* 16 (2016) 1695–1703.
- [4] X.F. Wang, Q. Liu, Y.Y. Bu, C.S. Liu, T. Liu, X.H. Yan, Optical temperature sensing of rare-earth ion doped phosphors, *RSC Adv.* 5 (2015) 86219–86236.
- [5] L. Marciak, K. Prorok, L. Francés-Sorianó, J. Pérez-Prieto, A. Bednarkiewicz, A broadening temperature sensitivity range with a core-shell YbEr/YbNd double ratiometric optical nanothermometer, *Nanoscale* 8 (2016) 5037–5042.
- [6] S.A. Wade, S.F. Collins, G.W. Baxter, Fluorescence intensity ratio technique for optical fiber point temperature sensing, *J. Appl. Phys.* 94 (2003) 4743–4756.
- [7] W. Tang, S.C. Wang, Z.L. Li, Y. Sun, L.M. Zheng, R. Zhang, B. Yang, W.W. Cao, M. Yu, Ultrahigh-sensitive optical temperature sensing based on ferroelectric Pr^{3+} -doped $(\text{K}_{0.5}\text{Na}_{0.5})\text{NbO}_3$, *Appl. Phys. Lett.* 108 (2016), 061902–1–061902–5.
- [8] P. Du, L.H. Luo, H.K. Park, J.S. Yu, Citric-assisted sol-gel based $\text{Er}^{3+}/\text{Yb}^{3+}$ -codoped $\text{Na}_{0.5}\text{Gd}_{0.5}\text{MoO}_4$: a novel highly-efficient infrared-to-visible upconversion material for optical temperature sensors and optical heaters, *Chem. Eng. J.* 306 (2016) 840–848.
- [9] L. Marciak, A. Pilch, S. Arabasz, D.Y. Jin, A. Bednarkiewicz, Heterogeneously Nd^{3+} doped single nanoparticles for NIR-induced heat conversion, luminescence, and thermometry, *Nanoscale* 9 (2017) 8288–8297.
- [10] A.S. Souza, L.A.O. Nunes, I.G.N. Silva, F.A.M. Oliveira, L.L. da Luz, H.F. Brito, M.C.F.C. Felinto, R.A.S. Ferreira, S.A. Júnior, L.D. Carlos, O.L. Malta, Highly-sensitive Eu^{3+} ratiometric thermometers based on excited state absorption with predictable calibration, *Nanoscale* 8 (2016) 5327–5333.
- [11] B.P. Singh, A.K. Parchur, R.S. Ningthoujam, P.V. Ramakrishna, S. Singh, P. Singh, S.B. Rai, R. Maalej, Enhanced up-conversion and temperature-sensing behaviour of Er^{3+} and Yb^{3+} co-doped $\text{Y}_2\text{Ti}_2\text{O}_7$ by incorporation of Li^+ ions, *Phys. Chem. Chem. Phys.* 16 (2014) 22665–22676.
- [12] R. Dey, V.K. Rai, Yb^{3+} sensitized Er^{3+} doped La_2O_3 phosphor in temperature sensors and display devices, *Dalton Trans.* 43 (2014) 111–118.
- [13] B. Dong, B.S. Cao, Y.Y. He, Z. Liu, Z.P. Li, Z.Q. Feng, Temperature sensing and *in vivo* imaging by molybdenum sensitized visible upconversion luminescence of rare-earth oxides, *Adv. Mater.* 24 (2012) 1987–1993.
- [14] S.F. León-Luis, U.R. Rodríguez-Mendoza, P. Haro-González, I.R. Martín, V. Lavín, Role of the host matrix on the thermal sensitivity of Er^{3+} luminescence in optical temperature sensors, *Sensors Actuators B. Chem.* 174 (2012) 176–186.
- [15] D. He, C. Guo, S. Jiang, N. Zhang, C. Duan, M. Yin, T. Li, Optical temperature sensing properties of Yb^{3+} - Er^{3+} co-doped NaLnTiO_4 ($\text{Ln} = \text{Gd}, \text{Y}$) upconversion phosphors, *RSC Adv.* 5 (2015) 1385–1390.
- [16] L.Z. Zhang, H.F. Lin, G. Zhang, X. Mateos, J.M. Serres, M. Aguiló, F. Diaz, U. Griebner, V. Petrov, Y.C. Wang, Crystal growth, optical spectroscopy and laser action of Tm^{3+} -doped monoclinic magnesium tungstate, *Opt. Express* 25 (2017) 3682–3693.
- [17] C.S. Lim, Microwave sol-gel process of $\text{KGd}(\text{WO}_4)_2:\text{Ho}^{3+}/\text{Yb}^{3+}$ phosphors and their upconversion photoluminescence properties, *J. Phys. Chem. Solids* 78 (2015) 65–69.
- [18] W. Xu, X.Y. Gao, L.J. Zheng, P. Wang, Z.G. Zhang, W.W. Cao, Optical thermometry through green upconversion emissions in $\text{Er}^{3+}/\text{Yb}^{3+}$ -codoped CaWO_4 phosphor, *Appl. Phys. Express* 5 (2012), 072201–1–072201–3.
- [19] H.Y. Lu, R. Meng, H.Y. Hao, Y.F. Bai, Y.C. Gao, Y.L. Song, Y.X. Wang, X.R. Zhang, Stark sublevels of $\text{Er}^{3+}/\text{Yb}^{3+}$ codoped $\text{Gd}_2(\text{WO}_4)_3$ phosphor for enhancing the sensitivity of a luminescent thermometer, *RSC Adv.* 6 (2016) S7667–S7671.
- [20] X.N. Chai, J. Li, X.S. Wang, Y.X. Li, X. Yao, Color-tunable upconversion photoluminescence and highly performed optical temperature sensing in $\text{Er}^{3+}/\text{Yb}^{3+}$ co-doped ZnWO_4 , *Opt. Express* 24 (2016) 22438–22447.
- [21] C. Cascales, C.L. Páino, E. Bazán, C. Zaldo, Ultrasmall, water dispersible, TWEEN80 modified $\text{Yb:Er:NaGd}(\text{WO}_4)_2$ nanoparticles with record

- upconversion ratiometric thermal sensitivity and their internalization by mesenchymal stem cells, *Nanotechnology* 28 (2017), 185101–1–185101–11.
- [22] M. Pollnau, D.R. Gamelin, S.R. Lüthi, H.U. Güdel, M.P. Hehlen, Power dependence of upconversion luminescence in lanthanide and transition-metal-ion systems, *Phys. Rev. B* 61 (2001) 3337–3346.
- [23] J. Feenstra, I.F. Six, M.A.H. Asselbergs, R.H. van Leest, J. de Wild, A. Meijerink, R.E.I. Schropp, A.E. Rowan, J.J. Schermer, Er³⁺/Yb³⁺ upconverters for InGaP solar cells under concentrated broadband illumination, *Phys. Chem. Chem. Phys.* 17 (2015) 11234–11243.
- [24] G.Y. Chen, T.Y. Ohulchansky, A. Kachynski, H. Agren, P.N. Prasad, Intense visible and near-infrared upconversion photoluminescence in colloidal LiYF₄: Er³⁺ nanocrystals under excitation at 1490 nm, *ACS Nano* 5 (2011) 4981–4986.
- [25] F.X. Wang, F. Song, G. Zhang, Y.D. Han, Q. Li, C.G. Ming, J.G. Tian, Upconversion and pump saturation mechanisms in Er³⁺/Yb³⁺ codoped Y₂Ti₂O₇ nanocrystals, *J. Appl. Phys.* 115 (2014), 134310–134311–134310–7.
- [26] G. Zhang, F. Song, C.G. Ming, Y. Yu, C. Zhang, H.Y. Zhao, Q.R. Wang, J.D. Liu, Photoluminescence properties and pump-saturation effect of Er³⁺/Yb³⁺ codoped Y₂Ti₂O₇ nanocrystals, *J. Lumin.* 132 (2012) 774–779.
- [27] T. Grzyb, A. Tymiński, Up-conversion luminescence of GdOF: Yb³⁺, Ln³⁺ (Ln = Ho, Tm, Er) nanocrystals, *J. Alloys Compd.* 660 (2016) 235–243.
- [28] A.K. Soni, V.K. Rai, Thermal and pump power effect in SrMoO₄:Er³⁺-Yb³⁺ phosphor for thermometry and optical heating, *Chem. Phys. Lett.* 667 (2017) 226–232.
- [29] R.D. Shannon, *Acta Cryst. A* 32 (1976) 751–767.
- [30] F. Huang, Y. Gao, J.C. Zhou, J. Xu, Y.S. Wang, Yb³⁺/Er³⁺ codoped CaMoO₄: a promising green upconversion phosphor for optical temperature sensing, *J. Alloys Compd.* 639 (2015) 325–329.
- [31] G. Lakshminarayana, J.R. Qiu, M.G. Brikk, G.A. Kumar, I.V. Kityk, Spectral analysis of Er³⁺, Er³⁺/Yb³⁺ and Er³⁺/Tm³⁺/Yb³⁺ doped TeO₂-ZnO-WO₃-TiO₂-Na₂O glasses, *J. Phys. Condens. Matter* 20 (2008), 375101–1–375101–8.
- [32] B.R. Judd, Optical Absorption intensity of rare-earth ions, *Phys. Rev.* 127 (1962) 750–761.
- [33] G.S. Ofelt, Intensities of crystal spectra of rare-earth ions, *J. Chem. Phys.* 37 (1962) 511–520.
- [34] H. Desirena, E. De la Rosa, L.A. Díaz-Torres, G.A. Kumar, Concentration effect of Er³⁺ ion on the spectroscopic properties of Er³⁺ and Yb³⁺/Er³⁺ co-doped phosphate glasses, *Opt. Mater.* 28 (2006) 560–568.
- [35] E. Maurice, G. Monnom, B. Dussardier, A. Saïssy, D.B. Ostrowsky, G.W. Baxter, Erbium-doped silica fibers for intrinsic fiber-optic temperature sensors, *Appl. Opt.* 34 (1995) 8019–8025.
- [36] L. Li, C.F. Guo, S. Jiang, D.K. Agrawal, T. Li, Green up-conversion luminescence of Yb³⁺-Er³⁺ co-doped CaLa₂ZnO₅ for optically temperature sensing, *RSC Adv.* 4 (2014) 6391–6396.
- [37] Z.Y. Zhang, C.F. Guo, H. Suo, X.Q. Zhao, N.M. Zhang, T. Li, Thermometry and up-conversion luminescence of Yb³⁺-Er³⁺ co-doped Na₂Ln₂Ti₃O₁₀ (Ln = Gd, La) phosphors, *Phys. Chem. Chem. Phys.* 18 (2016) 18828–18834.
- [38] S.S. Wang, H. Zhou, X.X. Wang, A.L. Pan, Up-conversion luminescence and optical temperature-sensing properties of Er³⁺-doped perovskite Na_{0.5}Bi_{0.5}TiO₃ nanocrystals, *J. Phys. Chem. Solids* 98 (2016) 28–31.
- [39] T.V. Gavrilovic, D.J. Jovanovic, V. Lojpur, M.D. Dramicanin, Multifunctional Eu³⁺- and Er³⁺/Yb³⁺-doped GdVO₄ nanoparticles synthesized by reverse-micelle method, *Sci. Rep.* 4 (2014).
- [40] X.N. Chai, J. Li, Y. Zhang, X.S. Wang, Y.X. Li, X. Yao, Bright dual-mode green emission and temperature sensing properties in Er³⁺/Yb³⁺ co-doped MgWO₄ phosphor, *RSC Adv.* 6 (2016) 64072–64078.
- [41] Z. Wei, W. Zheng, Z.Y. Zhu, X.F. Guo, Upconversion of SrWO₄: Er³⁺/Yb³⁺: improvement by Yb³⁺ codoping and temperature sensitivity for optical temperature sensors, *Chem. Phys. Lett.* 651 (2016) 46–49.
- [42] P. Du, L.L. Luo, J.S. Yu, Infrared-to-visible upconversion emission of Er³⁺/Yb³⁺-codoped SrMoO₄ phosphors as wide-range temperature sensor, *Curr. Appl. Phys.* 15 (2015) 1576–1579.
- [43] P. Du, L.H. Luo, J.S. Yu, Upconversion emission, cathodoluminescence and temperature sensing behaviors of Yb³⁺ ions sensitized NaY(WO₄)₂:Er³⁺ phosphors, *Ceram. Int.* 42 (2016) 5635–5641.
- [44] X. F. Wang, Y. Wang, J. Marques-Hueso, X. H. Yan, Improving Optical temperature sensing performance of Er³⁺ doped Y₂O₃ microtubes via co-doping and controlling excitation power, *Sci. Rep.* doi:10.1038/s41598-017-00838-w.
- [45] X.Z. Zhou, B.E. Smith, P.B. Roder, P.J. Pauzauskie, Laser refrigeration of ytterbium-doped sodium-yttrium-fluoride nanowires, *Adv. Mater.* 28 (2016) 8658–8662.
- [46] R. Dey, A. Pandey, V.K. Rai, Er³⁺-Yb³⁺ and Eu³⁺-Er³⁺-Yb³⁺ codoped Y₂O₃ phosphors as optical heater, *Sensors Actuators B Chem.* 1901 (2014) 512–515.
- [47] X.H. Xu, W.F. Zhang, D.C. Yang, W. Lu, J.B. Qiu, S.F. Yu, Phonon-assisted population inversion in lanthanide-doped upconversion Ba₂LaF₇ Nanocrystals in glass-ceramics, *Adv. Mater.* 28 (2016) 8045–8050.
- [48] C.J. da Silva, M.T. de Araujo, E.A. Gouveia, A.S. Gouveia-Neto, Thermal effect on multiphonon-assisted anti-Stokes excited upconversion fluorescence emission in Yb³⁺ sensitized Er³⁺ doped optical fiber, *Appl. Phys. B* 70 (2000) 185–188.
- [49] M.J. Weber, Multiphonon relaxation of rare earth ions in Yttrium Orthoaluminate, *Phys. Rev. B* 8 (1973) 54–64.